Title
Technical Note: A Monte Carlo study of magnetic-field-induced radiation dose effects in mice

Journal
Medical Physics, 42(9)

ISSN
0094-2405

Authors
Rubinstein, Ashley E
Liao, Zhongxing
Melancon, Adam D
et al.

Publication Date
2015-08-26

DOI
10.1118/1.4928600

Technical Note: A Monte Carlo study of magnetic-field-induced radiation dose effects in mice

Ashley E. Rubinstein
Department of Radiation Physics, The University of Texas MD Anderson Cancer Center, Houston, Texas 77030 and The University of Texas Graduate School of Biomedical Sciences, Houston, Texas 77030

Zhongxing Liao
Department of Radiation Oncology, The University of Texas MD Anderson Cancer Center, Houston, Texas 77030

Adam D. Melancon
Department of Radiation Physics, The University of Texas MD Anderson Cancer Center, Houston, Texas 77030

Michele Guindani
Department of Biostatistics, The University of Texas MD Anderson Cancer Center, Houston, Texas 77030

David S. Followill and Ramesh C. Tailor
Department of Radiation Physics, The University of Texas MD Anderson Cancer Center, Houston, Texas 77030

John D. Hazle
Department of Imaging Physics, The University of Texas MD Anderson Cancer Center, Houston, Texas 77030

Laurence E. Court[a)]
Departments of Radiation Physics and Imaging Physics, The University of Texas MD Anderson Cancer Center, Houston, Texas 77030

(Received 9 March 2015; revised 28 July 2015; accepted for publication 4 August 2015; published 26 August 2015)

Purpose: Magnetic fields are known to alter radiation dose deposition. Before patients receive treatment using an MRI-linear accelerator (MRI-Linac), preclinical studies are needed to understand the biological consequences of magnetic-field-induced dose effects. In the present study, the authors sought to identify a beam energy and magnetic field strength combination suitable for preclinical murine experiments.
Methods: Magnetic field dose effects were simulated in a mouse lung phantom using various beam energies (225 kVp, 350 kVp, 662 keV [Cs-137], 2 MV, and 1.25 MeV [Co-60]) and magnetic field strengths (0.75, 1.5, and 3 T). The resulting dose distributions were compared with those in a simulated human lung phantom irradiated with a 6 or 8 MV beam and orthogonal 1.5 T magnetic field.
Results: In the human lung phantom, the authors observed a dose increase of 45% and 54% at the soft-tissue-to-lung interface and a dose decrease of 41% and 48% at the lung-to-soft-tissue interface for the 6 and 8 MV beams, respectively. In the mouse simulations, the magnetic fields had no measurable effect on the 225 or 350 kVp dose distribution. The dose increases with the Cs-137 beam for the 0.75, 1.5, and 3 T magnetic fields were 9%, 29%, and 42%, respectively. The dose decreases were 9%, 21%, and 37%. For the 2 MV beam, the dose increases were 16%, 33%, and 31% and the dose decreases were 9%, 19%, and 30%. For the Co-60 beam, the dose increases were 19%, 54%, and 44%, and the dose decreases were 19%, 42%, and 40%.
Conclusions: The magnetic field dose effects in the mouse phantom using a Cs-137, 3 T combination or a Co-60, 1.5 or 3 T combination most closely resemble those in simulated human treatments with a 6 MV, 1.5 T MRI-Linac. The effects with a Co-60, 1.5 T combination most closely resemble those in simulated human treatments with an 8 MV, 1.5 T MRI-Linac. [http://dx.doi.org/10.1118/1.4928600]

Key words: MRI-Linac, Monte Carlo, magnetic fields, mice, radiation therapy

1. INTRODUCTION

The goal of creating increasingly precise, personalized treatments of cancer has led to the development of systems that integrate radiation therapy units with MRI. Various groups around the world have designed such systems for real-time imaging during radiation therapy delivery.[1–3] The integration of MRI with radiation therapy offers real-time tracking of tumors that move during treatment. These systems could also be used for real-time assessment of dose delivery and immediate adjustment of the treatment plan. Unfortunately, the MRI and radiation therapy systems in an integrated unit affect each other's function,[4–6] and concerns regarding radiation dosimetry and imaging distortions must be addressed before MRI-guided radiation therapy systems can be used clinically. The deposition of dose via ionizing radiation is

known to be altered by magnetic fields.[6–10] In the presence of a magnetic field, a moving charged particle is influenced by the Lorentz force, which causes the particle to curve in a direction perpendicular to both the magnetic field and instantaneous velocity vector. The particle's radius of curvature in a magnetic field is dependent on its kinetic energy and the strength of the magnetic field. Whereas a magnetic field will not affect the primary photon beam in radiation therapy, it will affect the dose-depositing secondary electrons.

Researchers at the University Medical Center Utrecht developed an MRI-linear accelerator (MRI-Linac) using a 1.5 T Achieva MRI scanner (Philips Healthcare, Best, the Netherlands) and an Elekta Linac (Elekta, Crawley, UK).[11] Early prototypes used a 6 MV Linac, but the most recent prototype uses an 8 MV Linac.[12] In treatments using this system, the beam from the Linac is oriented perpendicular to the magnetic field of the MRI. With this geometry, the MRI's magnetic field creates a laterally shifted, asymmetric dose profile. In inhomogeneous tissue, a phenomenon termed the electron return effect also comes into play.[9,13] This effect becomes important when secondary electrons transition from higher to lower density materials at interfaces such as the distal and lateral sides of a patient, air cavities, and the lung. The magnetic field's influence on radiation dose deposition can create hot and cold spots in these areas. These dose perturbations can be minimized in MRI-guided radiation therapy systems which orient the radiation beam parallel to the direction of the MRI's magnetic field.[14]

Monte Carlo simulations have demonstrated that for systems with a strong transverse magnetic field, irradiation of lung tissue surrounded by a higher density material will produce a dose increase at the high-to-low-density interface and a dose decrease at the low-to-high-density interface.[9,15] In previous studies, investigators simulated the irradiation of a human lung phantom with a 6 MV beam in the presence of a 1.5 T magnetic field. Raaijmakers *et al.*[9] used the Monte Carlo code GEANT4 to investigate magnetic field dose effects and found that the dose increased by 49% at the water-to-lung interface and decreased by 36% at the lung-to-water interface. Also, Kirkby *et al.*[15] performed simulations with the Monte Carlo codes PENELOPE and EGSnrc and observed an increase in the dose of up to 40% in the lung at the water-to-lung interface and a decrease in the dose of up to 26% in the lung at the lung-to-water interface.

Lung cancer patients often undergo radiation therapy, and because of the high radiosensitivity of the lung, these patients are at high risk for radiation-induced pneumonitis and fibrosis.[16] Typically, lung cancer patients have reduced lung function prior to treatment. Therefore, radiation-induced damage to healthy lung tissue can be especially problematic. MRI-Linacs have the potential to benefit lung cancer patients because of their real-time tumor tracking. However, hot and cold spots in the dose distribution may affect doses to lung lesions as well as healthy tissue, limiting the effectiveness of MRI-guided radiation therapy.

The precise therapeutic consequences of a magnetic field's influence on the spatial distribution of radiation dose is unknown. Therefore, preclinical studies are needed to ensure the safe clinical use of MRI-Linacs. To perform murine experiments for this purpose, the secondary electron range and radius of curvature in a magnetic field must be scaled down to mouse anatomy. In the study described herein, we sought to determine the optimal combination of beam energy and magnetic field strength required for preclinical murine experiments evaluating magnetic field dose effects in the lung. To that end, we simulated irradiation in the presence of a transverse magnetic field and compared the dose distributions in a mouse lung phantom with those in a human lung phantom. The beam energies used in these simulations were chosen to include orthovoltage beams produced by x-ray tubes in small animal irradiators (225 and 350 kVp), higher energy beams from radionuclide irradiators (662 keV [Cs-137] and 1.25 MeV [Co-60]), and a beam of an intermediate energy (2 MV). The kV beams were evaluated because, although the range of secondary electrons is very low, these are convenient beams for small animal irradiations. The higher energy beams were evaluated because, although they are less convenient for animal experiments, they are more likely to produce secondary electrons that will have the desired range and radius of curvature in a magnetic field.

2. METHODS

The Monte Carlo radiation transport code MCNP6 was used to simulate the effects of a magnetic field on radiation dose deposition in a mouse lung phantom. MCNP6 was developed by merging MCNP5 and MCNPX and is capable of tracking charged particles in magnetic fields in both void and material regions. In the present study, direct particle ray tracing in a magnetic field was implemented by adding a BFLD card to the input file to define a dipole field lying transverse to the radiation beam and adding a BFLCL card to the input file to define the regions to which the magnetic field was applied.[17]

Magnetic field dose effects were first examined in a human lung phantom with a 6 MV beam in the presence of a 1.5 T field in order to compare the resulting dose distributions to previously published data. Simulations were also run with an 8 MV beam as this is the energy of the newest prototype of the MRI-Linac. The simulation geometry was similar to that described by Raaijmakers *et al.*[9] and Kirkby *et al.*[15] A nondivergent 5×5-cm beam was delivered to a phantom composed of a 10-cm-thick slab of lung material surrounded by 4-cm-thick slabs of soft tissue material. For each of the beam energies, one simulation was run with no magnetic field present, and another was run with a 1.5 T field applied perpendicular to the direction of the photon beam. The composition data for the soft tissue and lung material used in this study were defined by NIST.[18] The density of the slabs of soft tissue material was 1.04 g/cm^3, whereas that of the slab of lung material was 0.26 g/cm^3.

The geometry for the mouse irradiation simulations is shown in Fig. 1. For each simulation, a 2.5×2.5-cm nondivergent photon beam was imparted on a 3.0×2.5×2.7-cm mouse lung phantom with a magnetic field applied perpendicular to the direction of the beam. The phantom consisted of a 0.6-cm

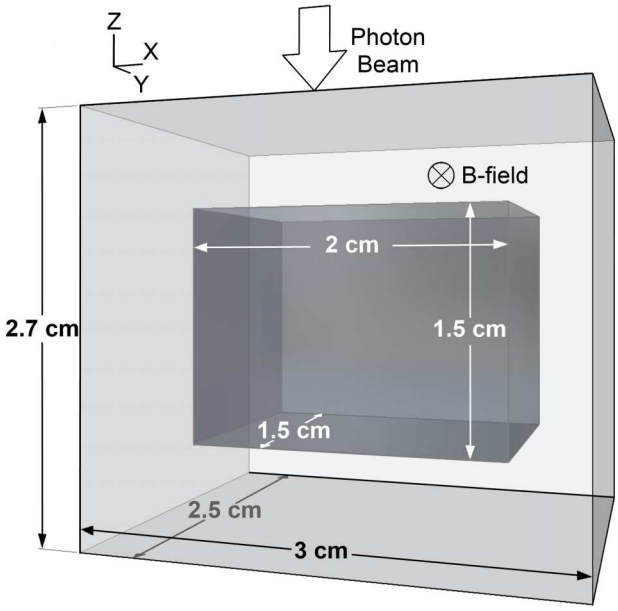

FIG. 1. Monte Carlo simulation geometry. The mouse lung phantom is composed of lung tissue (dark grey) surrounded by soft tissue (light grey). In the simulations, the phantom was irradiated from above in the z-direction with a 2.5×2.5-cm beam. A magnetic field was applied in the y-direction. Simulations were run using five different beams to irradiate the phantom in the absence of a magnetic field. Each simulation was then repeated for various magnetic field strengths.

slab of soft tissue, a 1.5-cm slab of lung tissue, and another 0.6-cm slab of soft tissue in the direction of the radiation beam. The phantom dimensions are representative of those in a mouse (as determined by cone-beam CT imaging of mice in our lab) with a few millimeters of buildup material added to the edges. The beam's field size was chosen to cover the entire lung, as whole-thorax irradiation is common in preclinical radiobiological studies. In these simulations, the magnetic field effects were examined using various beam energies (225 kVp, 350 kVp, 662 keV [Cs-137], 2 MV, and 1.25 MeV [Co-60]) and magnetic field strengths (0.75, 1.5, and 3 T).

The 225 and 350 kVp photon spectra were generated using the SpekCalc software program, which was designed to calculate the photon spectra from tungsten anode x-ray tubes.[19] The 225 kVp spectrum was created using the anode angle and filtration specified for the X-RAD 225Cx small animal irradiator (Precision X-Ray, North Branford, CT) (1.00 mm Cu HVL). The average energy of the beam was 86.5 keV. SpekCalc can only generate spectra for tube potentials of up to 300 keV. Therefore, the 350 kVp spectrum was estimated by first generating a photon spectrum from a highly filtered 300 kVp beam (3.80 mm Cu HVL). The spectrum was then modified by extending the high energy tail of the spectrum to include photon energies of up to 350 keV, resulting in 4% of the photons having energies between 300 and 350 keV. The resulting HVL of the beam was 3.95 mm Cu and the mean energy was 171 keV. Robar *et al.*[20] modeled an unflattened 2 MV beam from a 2100 C/D Linac (Varian Medical Systems, Palo Alto, CA) using the Monte Carlo code BEAM 2000. The authors described the photon energy spectrum for the simulated 2 MV beam; this spectrum was used in our simulations. The Cs-137 and Co-60 beams were simulated using monoenergetic photon sources of 662 keV and 1.25 MeV, respectively. For the 6 MV beam, the spectrum used was that described by Scarboro *et al.*,[21] which was calculated using an MCNPX model of a 6 MV Linac (Varian Medical Systems). The 8 MV spectrum used was that calculated by Ahnesjo and Andreo for an 8 MV beam produced by an SL75/20 machine (Philips Healthcare, Best, the Netherlands).[22]

The orthovoltage beam simulations (225 and 350 kVp) were run with 1×10^9 source histories, whereas the higher energy beam simulations were run with 100×10^6 source histories. In the human phantom simulations, the dose was tallied in $0.2\times1.0\times0.2$-cm voxels using the MCNP5-type mesh tally Fmesh4 (magnetic field tracking cannot be implemented in MCNPX mode[17]). The relative error of the dose tally was below 1%. For the mouse phantom simulations, the dose was tallied in voxels of $0.05\times0.05\times0.05$-cm and the relative error of the dose tally was below 5%. The error was larger in the mouse phantom simulations due to the smaller voxel size. To quantify magnetic field dose effects, local dose increases and decreases were calculated at the soft-tissue-lung interfaces. The dose increase to the lung at the soft-tissue-to-lung interface was calculated as

$$\frac{(D_{1.5}-D_0)}{D_0} \tag{1}$$

in which D_0 is the dose at the interface for the $B=0$ T case and $D_{1.5}$ is the dose at the same point for the $B=1.5$ T case. The dose decrease was defined as

$$\frac{(D_0-D_{1.5})}{D_0} \tag{2}$$

and was measured at the lung-to-soft-tissue interface. This method is slightly different from that used by Kirkby *et al.*[15] and Raaijmakers *et al.*,[9] who described the dose increase and decrease relative to the maximum dose for the $B=0$ T case. To compare our measured magnetic field dose effects with the results described by Kirkby and Raaijmakers, Eqs. (1) and (2) were used to recalculate dose increases and decreases using the depth-dose curves provided in those authors' publications (Table I).

3. RESULTS

After we completed the simulations of irradiation of a human lung phantom, we read out the dose along the central axis. The dose deposited under normal conditions ($B=0$ T) and in the presence of a 1.5 T field is plotted in Fig. 2(a). The dose was normalized to the maximum dose for the $B=0$ T case. For the 6 MV beam, we observed a dose increase of 45% in the lung near the soft-tissue-to-lung interface. At this interface, secondary electrons transition into the lower density lung tissue and are forced back toward the soft tissue by the Lorentz force. At the lung-to-soft-tissue interface, secondary electrons that would be turned around in the lung tissue instead enter the soft tissue, where they have a shorter range and are unable to return to the lung tissue. In our study, this

TABLE I. The dose increases at the soft-tissue-to-lung interface and dose decreases at the lung-to-soft-tissue interface during irradiation of human and mouse lung phantoms in the presence of a magnetic field.

Beam energy and magnetic field strength	Dose increase to the lung at the soft-tissue-to-lung interface (%)	Dose decrease to the lung at the lung-to-soft-tissue interface (%)
Human lung phantom		
6 MV, 1.5 T	45	41
6 MV, 1.5 T[a]	52	47
6 MV, 1.5 T[b]	45	37
8 MV, 1.5 T	54	48
Mouse lung phantom		
Cs-137, 0.75 T	9	9
Cs-137, 1.5 T	29	21
Cs-137, 3 T	42	37
2 MV, 0.75 T	16	9
2 MV, 1.5 T	33	19
2 MV, 3 T	31	30
Co-60, 0.75 T	19	19
Co-60, 1.5 T	54	42
Co-60, 3 T	44	40

[a]The values were calculated from Fig. 11 in the report by Raaijmakers *et al.* (Ref. 9).
[b]The values were calculated from Fig. 3 in the report by Kirkby *et al.* (Ref. 15).

effect caused a dose decrease of 41% at the lung-to-soft-tissue interface. For the 8 MV beam, we observed a 54% dose increase in the lung near the soft-tissue-to-lung interface and a 48% dose decrease in the lung near the lung-to-soft-tissue interface.

For each of the beam energies used in mouse lung phantom irradiations, we ran four simulations (one simulation for each magnetic field strength) and normalized the dose to the maximum dose for the $B = 0$ T case. Dose maps for the 350 kVp, Cs-137, 2 MV, and Co-60 beams are shown in Fig. 3. The dose maps for the 225 kVp beam resembled those for the 350 kVp beam. At the orthovoltage beam energies, the magnetic fields had no effect on the dose distributions except for an increase in the dose to the last voxel of the phantom and to the air immediately distal to the far edge of the phantom. For the Cs-137, 2 MV, and Co-60 beams, we observed a buildup of dose at the top and left side of the lung and a decrease in dose at the bottom and right side of the lung when we applied a 0.75 T magnetic field. Increasing the magnetic field strength caused the hot and cold spots to shift in a clockwise direction. At 0.75 T, we saw a lateral dose increase near the distal edge of the phantom owing to the relatively large trajectory radius of dose-depositing electrons. This effect decreased with an increase in magnetic field strength. For each of the magnetic fields, increasing the energy caused the extent of the magnetic field dose effects to increase. However, increasing the magnetic field strength caused the extent of the dose effects to decrease. For the Cs-137 beam, the dose increases to the lung at the soft-tissue-to-lung interface for the 0.75, 1.5, and 3 T magnetic fields were 9%, 29%, and 42%, respectively, and the dose decreases to the lung at the lung-to-soft-tissue interface were 9%, 21%, and 37%, respectively [Fig. 2(b)]. For the 2 MV beam, the dose increases were 16%, 33%, and 31%, and the dose decreases were 9%, 19%, and 30% [Fig. 2(c)]. For the Co-60 beam, the dose increases were 19%, 54%, and 44%, and the dose decreases were 19%, 42%, and 40% [Fig. 2(d)]. These results are summarized in Table I.

4. DISCUSSION

Our Monte Carlo simulations demonstrated that varying the beam energy and magnetic field strength can greatly affect both the location and magnitude of magnetic field dose effects in a mouse lung phantom. These effects vary with the range, radius of curvature, and average direction of dose-depositing secondary electrons within a magnetic field. In our simulations, the magnetic fields had no measureable effect on the 225 or 350 kVp dose distributions except for a slight dose increase at the distal phantom-to-air interface. This is likely because the range of low-energy electrons in the lung is very short, so the electrons stop before returning to the soft tissue. However, upon entering air, the electron range increases enough for the Lorentz force to force them back toward the phantom. Current small animal radiation therapy units typically have energies in the orthovoltage range, and owing to the short range of secondary electrons produced by these systems, their use in magnetic field dose effect studies is very limited.

Increasing the energy of the primary photon beam increases the range of the secondary electrons, and the longer the range of the electrons, the more the dosimetry will be influenced by the magnetic field. As the energy of the beam increases, the secondary electron radius of curvature also increases. With increased energy, the electrons are more likely to enter the lung and be turned around in the magnetic field, redepositing the dose in tissue. Increasing the magnetic field strength causes the trajectory radius of electrons to decrease. Additionally, as Raaijmakers *et al.*[9] pointed out, the average direction of electrons becomes more horizontal as the magnetic field strength increases, which influences the resulting dose distributions.

Raaijmakers *et al.*[9] studied the magnetic field dose effects for a 6 MV beam and magnetic field strengths of 0.2–3.0 T around cylindrical air cavities. In their study, the dose distributions were influenced by the trajectory radius and average direction of the electrons. However, the electron range was not a factor, as they used only one beam energy. Additionally, the electrons in their study traversed a cavity of air, whereas ours traversed a section of the lung. Despite these differences between the two studies, they had similar trends in resulting dose distributions. In both studies, the areas of reduced and increased dose rotated clockwise around the lower density region as the magnetic field strength increased. This rotation results from a change in the average direction of electrons from mostly downward at 0.75 T to mostly lateral at 3 T. Another similarity between the dose distributions in the two studies is that the extent of magnetic field dose effects decreased as the magnetic field strength increased. We saw the same effect as we decreased the beam energy in the simulations. Lowering the beam energy and raising

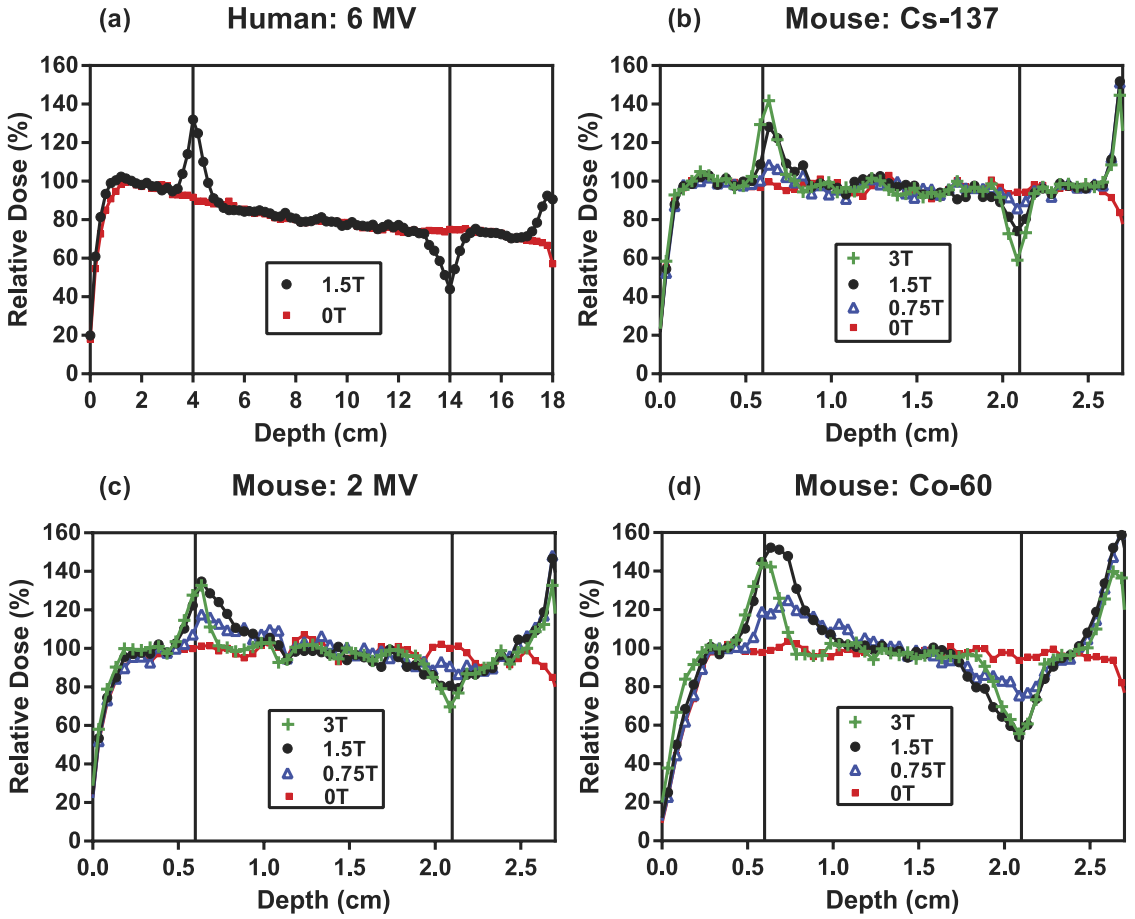

FIG. 2. Central axis percent depth-dose curves for (a) a 6 MV beam in a human phantom and for (b) Cs-137 (662 keV), (c) 2 MV, and (d) Co-60 (1.25 MeV) beams in a mouse phantom. The vertical black lines represent the soft-tissue-to-lung interface (left) and lung-to-soft-tissue interface (right). For each of the beam energies, the doses at magnetic field strengths of 0.75, 1.5, and 3 T are relative to the D_{max} for the $B = 0$ T case. Although the mouse phantom was an order of magnitude smaller than the human phantom, the depth-dose curves for the two phantoms were comparable. In both phantoms, the addition of a magnetic field caused a dose increase at the interface between the first slab of soft tissue and the lung and a dose decrease as the beam left the lung and entered the second slab of soft tissue.

the magnetic field strength likely cause hot and cold spots to become more localized because both actions reduce the electron trajectory radius. Additionally, decreasing the beam energy reduces the range of the electrons, confining them to a smaller region and localizing the magnetic field dose effects.

It is important to note that MCNP6 has not been experimentally benchmarked with respect to its dosimetry in the presence of a magnetic field. However, the results of our human phantom simulations fall between those measured by Raaijmakers *et al.*[9] and Kirkby *et al.*,[15] (Table I). We used the same phantom geometry (10 cm of lung surrounded by 4 cm of soft tissue) and the same voxel size ($0.2 \times 1.0 \times 0.2$-cm) as Kirkby *et al.* The difference in the results could be due to differences in spectra or the fact that we used slabs of NIST-defined soft tissue material while they used slabs of water on either sides of the lung. The magnitude of the magnetic-field-induced dose effects described by Raaijmakers *et al.* was larger than that of our study. This could be due to differences in spectra, differences in geometry (they used 8 cm of lung surrounded by 4 cm of water), or differences in voxel size (they used $0.05 \times 0.05 \times 0.05$-cm voxels).

The choice of beam energy and magnetic field strength used in preclinical studies to determine the biological consequences of magnetic field dose effects will depend on the magnetic field strength, the beam energy, and the geometry of the clinical system under investigation. It will also depend on the size of the animal model. In the present study, we sought to produce dose distributions in mice that were comparable with the dose distributions seen in humans given treatment with an MRI-Linac using a 6 or 8 MV beam in the presence of a transverse 1.5 T magnetic field. There are currently two other workable MRI-guided radiation therapy systems: the Linac-MR system[23] (6 MV, 0.5 T) at the Cross Cancer Institute and the ViewRay system[1] (Co-60, 0.35 T). These systems have not been included in our study because they avoid dose perturbations at soft-tissue-lung interfaces by orienting the magnetic field parallel to the radiation beam or by using low magnetic field strengths.[14,23–25]

Table I demonstrates that the magnitude of the dose increases and decreases in a mouse lung phantom most closely resemble that in a human lung phantom for a 6 MV beam and 1.5 T field when a Cs-137 beam and 3 T field or a Co-60 beam and 1.5 or 3 T field are used (within 15%). The magnitude of the dose increases and decreases in a mouse lung phantom most closely resemble that in a human lung phantom for an 8 MV beam and 1.5 T field when a Co-60 beam and a 1.5 T field

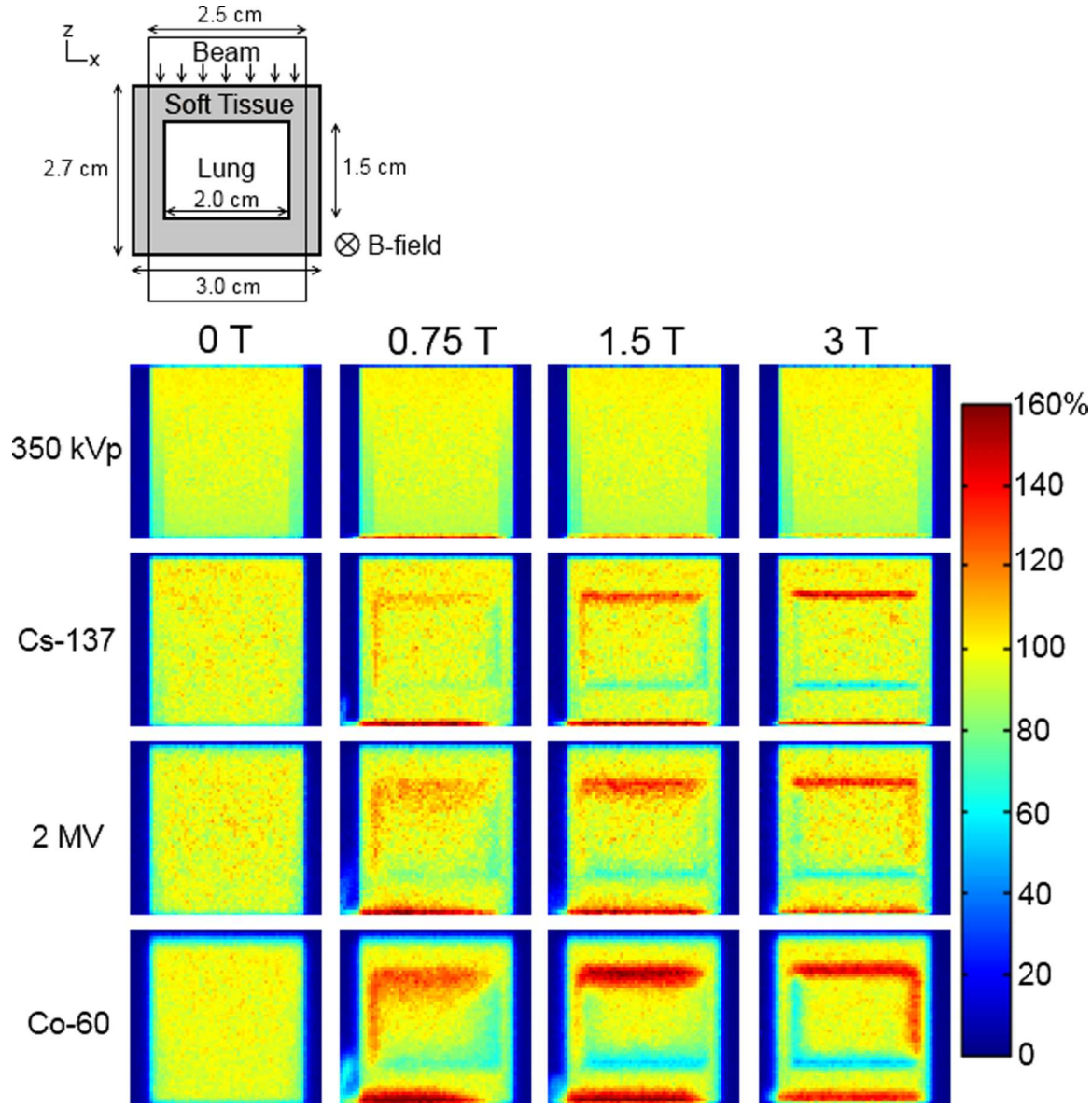

FIG. 3. Dose maps for irradiation of a mouse lung phantom with different beam energy/magnetic field strength combinations. The schematic at the top of the figure shows the simulation geometry. The magnetic field is perpendicular to the plane of the schematic and dose maps. Each row shows dose distributions for a particular beam energy with magnetic fields of 0, 0.75, 1.5, and 3 T. The 250 kVp beam dose maps looked similar to the 350 kVp dose maps (i.e., application of a magnetic field caused no dose perturbations except at the distal phantom-to-air interface).

are used. The magnitude of magnetic field dose effects that would be produced by a combination not used in our study can be estimated by interpolation of the data in Table I.

In Monte Carlo studies, the choice of voxel size can affect the quantification of magnetic-field-induced dose perturbations.[26] If the voxels are large relative to the range and radius of curvature of the secondary electrons, volume averaging will reduce the magnitude of magnetic field dose effects. In order to determine whether our chosen voxel size was adequate, we ran a mouse phantom simulation using the Cs-137 beam and a 3 T field with $0.03 \times 0.03 \times 0.03$-cm voxels, reducing the volume of the voxels by nearly 80%. In this simulation, we found that the maximum dose at the soft-tissue-to-lung interface was only 2% higher than it was in the simulation with $0.05 \times 0.05 \times 0.05$-cm voxels. Decreasing the size of the voxels affected the dose to the lung voxel at the lung-to-soft-tissue interface by less than 0.5%. Based on the results of this simulation, we would not expect that reducing the voxel size of the mouse phantom simulations would change our conclusions.

5. CONCLUSION

Before cancer patients undergo treatment with an MRI-Linac or other MRI-guided radiation therapy platform, the biological consequences of magnetic-field-induced dose effects must be understood. Based on the results of our study, we recommend using a Cs-137 beam and 3 T magnetic field or a Co-60 beam and 1.5 or 3 T field in preclinical murine experiments investigating magnetic field dose effects

produced by a 6 MV, 1.5 T MRI-Linac. To investigate magnetic field dose effects produced by an 8 MV, 1.5 T MRI-Linac, we recommend using a Co-60 beam and a 1.5 T field. With these beam energy and magnetic field strength combinations, the magnetic-field-induced dose effects in mice can resemble those in humans given treatment with a 6 or 8 MV, 1.5 T MRI-Linac.

ACKNOWLEDGMENT

This work was partially funded by Elekta.

[a]Author to whom correspondence should be addressed. Electronic mail: lecourt@mdanderson.org; Telephone: 713-563-2546.

[1]S. Mutic and J. F. Dempsey, "The ViewRay system: Magnetic resonance-guided and controlled radiotherapy," Semin. Radiat. Oncol. **24**, 196–199 (2014).
[2]J. J. Lagendijk, B. W. Raaymakers, and M. van Vulpen, "The magnetic resonance imaging-Linac system," Semin. Radiat. Oncol. **24**, 207–209 (2014).
[3]B. G. Fallone, B. Murray, S. Rathee, T. Stanescu, S. Steciw, S. Vidakovic, E. Blosser, and D. Tymofichuk, "First MR images obtained during megavoltage photon irradiation from a prototype integrated Linac-MR system," Med. Phys. **36**, 2084–2088 (2009).
[4]A. Ganguly, Z. Wen, B. L. Daniel, K. Butts, S. T. Kee, V. Rieke, H. M. Do, N. J. Pelc, and R. Fahrig, "Truly hybrid X-ray/MR imaging: Toward a streamlined clinical system," Acad. Radiol. **12**, 1167–1177 (2005).
[5]B. Burke, K. Wachowicz, B. G. Fallone, and S. Rathee, "Effect of radiation induced current on the quality of MR images in an integrated Linac-MR system," Med. Phys. **39**, 6139–6147 (2012).
[6]B. W. Raaymakers, A. J. E. Raaijmakers, A. N. T. J. Kotte, D. Jette, and J. J. W. Lagendijk, "Integrating a MRI scanner with a 6 MV radiotherapy accelerator: Dose deposition in a transverse magnetic field," Phys. Med. Biol. **49**, 4109–4118 (2004).
[7]A. J. Raaijmakers, B. W. Raaymakers, and J. J. Lagendijk, "Experimental verification of magnetic field dose effects for the MRI-accelerator," Phys. Med. Biol. **52**, 4283–4291 (2007).
[8]A. J. Raaijmakers, B. W. Raaymakers, S. van der meer, and J. J. Lagendijk, "Integrating a MRI scanner with a 6 MV radiotherapy accelerator: Impact of the surface orientation on the entrance and exit dose due to the transverse magnetic field," Phys. Med. Biol. **52**, 929–939 (2007).
[9]A. J. Raaijmakers, B. W. Raaymakers, and J. J. Lagendijk, "Magnetic-field-induced dose effects in MR-guided radiotherapy systems: Dependence on the magnetic field strength," Phys. Med. Biol. **53**, 909–923 (2008).
[10]D. P. Whitmire, D. L. Bernard, M. D. Peterson, and J. A. Purdy, "Magnetic enhancement of electron dose distribution in a phantom," Med. Phys. **4**, 127–131 (1977).
[11]B. W. Raaymakers, J. J. Lagendijk, J. Overweg, J. G. Kok, A. J. Raaijmakers, E. M. Kerkhof, R. W. van der Put, I. Meijsing, S. P. Crijns, F. Benedosso, M. van Vulpen, C. H. de Graaff, J. Allen, and K. J. Brown, "Integrating a 1.5 T MRI scanner with a 6 MV accelerator: Proof of concept," Phys. Med. Biol. **54**, N229–N237 (2009).
[12]C. Kontaxis, G. H. Bol, J. J. Lagendijk, and B. W. Raaymakers, "Towards adaptive IMRT sequencing for the MR-Linac," Phys. Med. Biol. **60**, 2493–2509 (2015).
[13]A. J. Raaijmakers, B. W. Raaymakers, and J. J. Lagendijk, "Integrating a MRI scanner with a 6 MV radiotherapy accelerator: Dose increase at tissue-air interfaces in a lateral magnetic field due to returning electrons," Phys. Med. Biol. **50**, 1363–1376 (2005).
[14]C. Kirkby, B. Murray, S. Rathee, and B. G. Fallone, "Lung dosimetry in a Linac-MRI radiotherapy unit with a longitudinal magnetic field," Med. Phys. **37**, 4722–4732 (2010).
[15]C. Kirkby, T. Stanescu, S. Rathee, M. Carlone, B. Murray, and B. G. Fallone, "Patient dosimetry for hybrid MRI-radiotherapy systems," Med. Phys. **35**, 1019–1027 (2008).
[16]G. Rodrigues, M. Lock, D. D'Souza, E. Yu, and J. Van Dyk, "Prediction of radiation pneumonitis by dose–volume histogram parameters in lung cancer—A systematic review," Radiother. Oncol. **71**, 127–138 (2004).
[17]J. Bull, "Magnetic field tracking features," MCNP6, Los Alamos National Laboratory, LA-UR-11–00872 (Los Alamos, NM, 2011).
[18]NIST, Composition of LUNG (ICRP), National Institute of Standards and Technology, Gaithersburg, MD, 2005 (available at http://physics.nist.gov/cgi-bin/Star/compos.pl?matno=190).
[19]G. Poludniowski, G. Landry, F. DeBlois, P. Evans, and F. Verhaegen, "SpekCalc: A program to calculate photon spectra from tungsten anode x-ray tubes," Phys. Med. Biol. **54**, N433–N438 (2009).
[20]J. L. Robar, S. A. Riccio, and M. Martin, "Tumour dose enhancement using modified megavoltage photon beams and contrast media," Phys. Med. Biol. **47**, 2433–2449 (2002).
[21]S. B. Scarboro, D. S. Followill, R. M. Howell, and S. F. Kry, "Variations in photon energy spectra of a 6 MV beam and their impact on TLD response," Med. Phys. **38**, 2619–2628 (2011).
[22]A. Ahnesjo and P. Andreo, "Determination of effective bremsstrahlung spectra and electron contamination for photon dose calculations," Phys. Med. Biol. **34**, 1451–1464 (1989).
[23]J. Yun, E. Yip, Z. Gabos, K. Wachowicz, S. Rathee, and B. G. Fallone, "Neural-network based autocontouring algorithm for intrafractional lung-tumor tracking using Linac-MR," Med. Phys. **42**, 2296–2310 (2015).
[24]H. O. Wooten, O. Green, M. Yang, T. DeWees, R. Kashani, J. Olsen, J. Michalski, D. Yang, K. Tanderup, Y. Hu, H. H. Li, and S. Mutic, "Quality of Intensity modulated radiation therapy treatment plans using a (60)Co magnetic resonance image guidance radiation therapy system," Int. J. Radiat. Oncol., Biol., Phys. **92**, 771–778 (2015).
[25]Y. M. Yang and B. Bednarz, "Consistency evaluation between EGSnrc and GEANT4 charged particle transport in an equilibrium magnetic field," Phys. Med. Biol. **58**, N47–N58 (2013).
[26]B. M. Oborn, P. E. Metcalfe, M. J. Butson, and A. B. Rosenfeld, "High resolution entry and exit Monte Carlo dose calculations from a linear accelerator 6 MV beam under the influence of transverse magnetic fields," Med. Phys. **36**, 3549–3559 (2009).